Int. J. Heat Mass Transfer. Vol. 36, No. 7, pp. 1993–1997, 1993
Printed in Great Britain

0017-9310/93 $6.00 + 0.00

TECHNICAL NOTES

Three-dimensional natural convection in a cubical enclosure with walls of finite conductance

TORU FUSEGI†
Institute of Computational Fluid Dynamics, 1-22-3 Haramachi, Meguro, Tokyo 152, Japan

JAE MIN HYUN
Department of Mechanical Engineering, Korea Advanced Institute of Science and Technology, Chong Ryang, Seoul 131, Korea

and

KUNIO KUWAHARA
Institute of Space and Astronautical Science, 3-1-1 Yoshinodai, Sagamihara, Kanagawa 229, Japan

(*Received* 4 *September* 1991 *and in final form* 9 *January* 1992)

INTRODUCTION

NATURAL convection in a side wall-heated enclosure, as shown schematically in Fig. 1, serves as a model for diverse types of thermal engineering systems. A large number of past investigations have dealt with this class of convective phenomena at high Rayleigh numbers by using a variety of theoretical, numerical and experimental techniques (see the reviews by, e.g. Ostrach [1]). For the basic laminar two-dimensional flows in an air-filled square cavity, benchmark numerical solutions are available for Rayleigh numbers up to $Ra = 10^8$ [2–4]. It is important to note the significance of the thermal boundary conditions at the bounding surface walls of the container. In the majority of prior studies, it has been customary to specify the completely insulated condition at the walls other than the isothermal vertical side walls. On the other hand, several two-dimensional numerical analyses [5–7] delineated the changes in the flow properties when the horizontal walls were perfect conductors. In essence, the adoption of a perfect conductor implies that the temperature itself, rather than the temperature gradient, is prescribed on the boundary wall of interest. As examples, the cases of a constant-temperature or a linearly varying temperature profile on the horizontal surfaces were examined in detail [5–7]. The results of these studies clearly identified that the gross flow and heat transfer characteristics were substantially affected by the precise forms of thermal conditions at the boundary walls.

For actual thermal systems, both the completely insulating condition and the perfect conducting condition represent highly idealized extreme situations. The realistic conditions at the solid boundary walls of a container may be better characterized as partially conducting; the solid walls are materials of finite thermal conductance. The temperature distribution at the solid walls is, therefore, not known *a priori*. An accurate determination of the thermal behavior at the walls constitutes a crucial part of the solution process of the problem.

It follows that an in-depth understanding of the convective heat transfer properties, with the introduction of more realistic thermal boundary conditions, is warranted. The present work addresses this aspect. The purpose of the present note is to illustrate the flow and thermal fields inside the container by using a physical model which incorporates the finiteness of thermal conductivity of the boundary solid walls.

One plausible approach would be to formulate a conjugate heat transfer problem. This involves a simultaneous treatment of conduction in the solid walls as well as convection in the fluid inside the container. Kim and Viskanta [8] successfully applied this methodology to two-dimensional rectangular enclosures. An air-filled cavity was fitted inside a square solid block, the external surfaces of which were heated differentially in either the vertical or horizontal direction. The conjugate heat transfer approach is straightforward since not much modification is required to the existing solution schemes designed for conventional convective fluid flows. However, due to the enlarged computational domain which now includes the solid walls, an appreciable increase of computational effort is unavoidable. This undercuts the attractiveness of the method, and the difficulties compound, especially when fully three-dimensional situations are under consideration.

A preferred alternative is to devise a model which would incorporate the effects of solid wall conductance to the boundary condition at the solid surfaces. This can be accomplished by introducing the concept of thermal conductance S, which is defined as

$$S^* \equiv \frac{k_s}{k_0} L_s^{-1} \tag{1}$$

where k_s and k_0 stand for the thermal conductivity of the solid wall and of fluid, respectively, and L_s refers to the thickness of the wall [9, 10]. Relying on this concept [9], the thermal boundary condition at e.g. $y^* = 0$, can be expressed as

$$\frac{\partial T^*}{\partial y^*} = S_y^*(T_e^* - T^*) \tag{2}$$

where the subscript y is affixed to S^* in order to denote the conductance of the horizontal wall. Similar expressions can be obtained for the other walls of the cavity. It is obvious that, by setting S_y^* equal to zero, the completely insulated condition is recovered. Note that the above formulation involves the temperature of the environment, T_e^*, to which the external surfaces of the container walls are exposed.

† To whom all correspondence should be addressed. Presently, Energy Technology Research Institute, Tokyo Gas Co, Ltd, 1-16-25 Shibaura, Minato, Tokyo 105, Japan.

NOMENCLATURE

c_p	specific heat at constant pressure [J kg^{-1} K^{-1}]
g	gravitational acceleration [m s^{-2}]
k_0, k_s	thermal conductivities of fluid and of wall, respectively [W K^{-1} m^{-1}]
L_0	reference length (enclosure width) [m]
L_s	thickness of wall [m]
$Nu, \overline{Nu}$	the local and average Nusselt numbers
Pr	Prandtl number, $c_p\mu/k_0$
Ra	Rayleigh number, $g\beta c_p\rho^2 L_0^3(T_H-T_C)/\mu k_0$
S_y, S_z	non-dimensional thermal conductance in the y- and z-directions, $(S_y^*, S_z^*)L_0$
T	non-dimensional temperature, $(T^*-T_C)/(T_H-T_C)$
T_C, T_H	temperatures of the cooled and the heated side walls, respectively [K]
T_e	non-dimensional environmental temperature, $(T_e^*-T_C)/(T_H-T_C)$
u_0	reference velocity, $[g\beta L_0(T_H-T_C)]^{1/2}$ [m s^{-1}]
u	non-dimensional velocity component in the x-direction, u^*/u_0
x, y, z	non-dimensional Cartesian coordinates, $(x^*, y^*, z^*)/L_0$.

Greek symbols

β	thermal expansion coefficient [K^{-1}]
μ	viscosity [kg m^{-1} s^{-1}]
ρ	density [kg m^{-3}].

Superscript

*	dimensional quantities.

In the present paper, the effects of finite conductance at the bounding walls of a cubical enclosure (sketched in Fig. 1) are delineated by numerically solving the governing equations. An air-filled cavity ($Pr = 0.71$) is considered. The side walls at $x^* = 0$ and L_0 are differentially heated at T_H and T_C ($T_H > T_C$), respectively. Results are acquired for $Ra = 10^6$. The field patterns at this Rayleigh number are representative of those observed for relatively high values of Ra; the boundary layers form near the isothermal side walls ($x^* = 0$ and L_0), and a near-stagnant core exists in the interior.

The present formulation, shown in (1) and (2), was conceived and effectively utilized in ref. [9] for various two-dimensional convective processes. The strength of this approach lies in its simplicity; yet, much of the relevant physics is represented in this model. As stated earlier, this model can, with virtually no extra cost for computations, simulate the conditions of the solid as well as the external environment. The thermal conductance is not necessarily a constant; it may vary in space as well as in time, which can accommodate the non-uniformity of the wall conditions. When specifying large S_y^* to simulate a situation with a highly conducting solid wall, the value of S_y^* may be adjusted properly near $y^* = 0$ and L_0 so that the present formulation could accurately handle the corner effects. However, in the present study, the thermal conductance is assumed to be constant and the range of S_y^* and S_z^* does not exceed 10.0.

A similar numerical investigation was documented recently by Le Pentrec and Lauriat [11]. Their work was focused to the effects of finite thermal conductance of the end walls ($z^* = 0$ and L_0) only. Two cases of the environmental temperature, namely $T_e^* = T_0$ or T_C, were examined for both air- and water-filled cavities in the range of $10^5 \leqslant Ra \leqslant 10^7$. For the case of air as the medium, notable three-dimensional

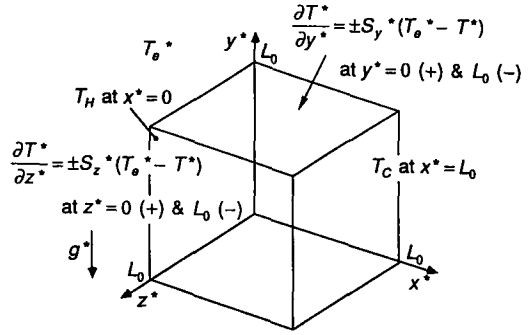

FIG. 1. The geometry and the boundary conditions of the problem.

variations appeared in the field near the end walls ($z^* = 0$ and L_0) when a relatively large conductance ($S_y^* > 10.0$) was assigned, together with the condition that $T_e^* = T_C$.

The main emphasis of the present study is placed on scrutinizing detailed local physical properties of the flow and temperature fields under the presence of partially conducting horizontal and end walls. Three-dimensional features of flow and heat transfer inside the cavity are illustrated by systematically altering the thermal conductance of the horizontal walls ($y^* = 0$ and L_0) and that of the end walls ($z^* = 0$ and L_0). Impacts of the environmental temperature on field patterns are also considered.

The present numerical work employs a large number of grid points, i.e. 62^3. In the case of perfectly insulated wall conditions ($S_y^* = S_z^* = 0.0$), the accuracy of the present three-dimensional results was proven to be comparable to that achieved by the most elaborate two-dimensional benchmark solutions documented in the literature [12].

The flow is governed by the three-dimensional, time-dependent, incompressible Navier–Stokes and energy equations. The Boussinesq approximation is invoked for the physical properties of fluid. These equations are solved by a control volume based finite difference procedure. The mathematical formulation and the numerical methodology are available elsewhere [12], and they are not repeated here. It suffices to mention that the convective terms are discretized by the QUICK scheme modified for non-uniform grids [13] and that the iterative solution algorithm is based on the well-known SIMPLE type [14] and the Strongly Implicit Procedure [15].

RESULTS AND DISCUSSION

The three-dimensional variations of field patterns are assessed by examining the distribution of the Nusselt number at the isothermal vertical side walls ($x = 0$ and 1). For this purpose, the local and average Nusselt numbers are defined, respectively, as

$$\text{the local Nusselt number: } Nu(y,z) = -\left.\frac{\partial T}{\partial x}\right|_{x=0 \text{ or } 1}$$

the average Nusselt number:

$$\overline{Nu} = \int_{y=0}^{y=1}\int_{z=0}^{z=1} Nu(y,z)\,dy\,dz. \quad (3)$$

Figures 2 and 3 display the distribution of the local Nusselt number at $x = 0$ for different values of S_y, S_z and T_e. In the results presented in Fig. 2, the environmental temperature T_e is equal to 0.5; consequently, the local Nusselt number distribution at the cooled wall (at $x = 1$) is anti-symmetric

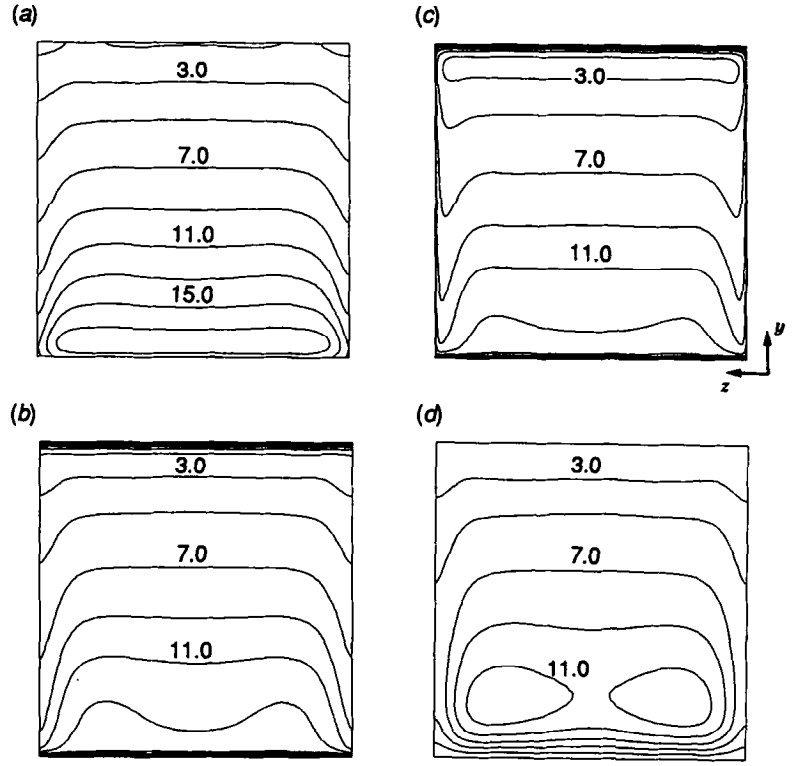

FIG. 2. The distribution of the local Nusselt number, Nu, at the heated wall ($x = 0$) for $Ra = 10^6$ and $T_c = 0.5$. (a) $S_y = S_z = 0.0$. (b) $S_y = 10.0$ and $S_z = 0.0$. (c) $S_y = 10.0$ and $S_z = 5.0$. (d) $S_y \to \infty$ and $S_z = 0.0$.

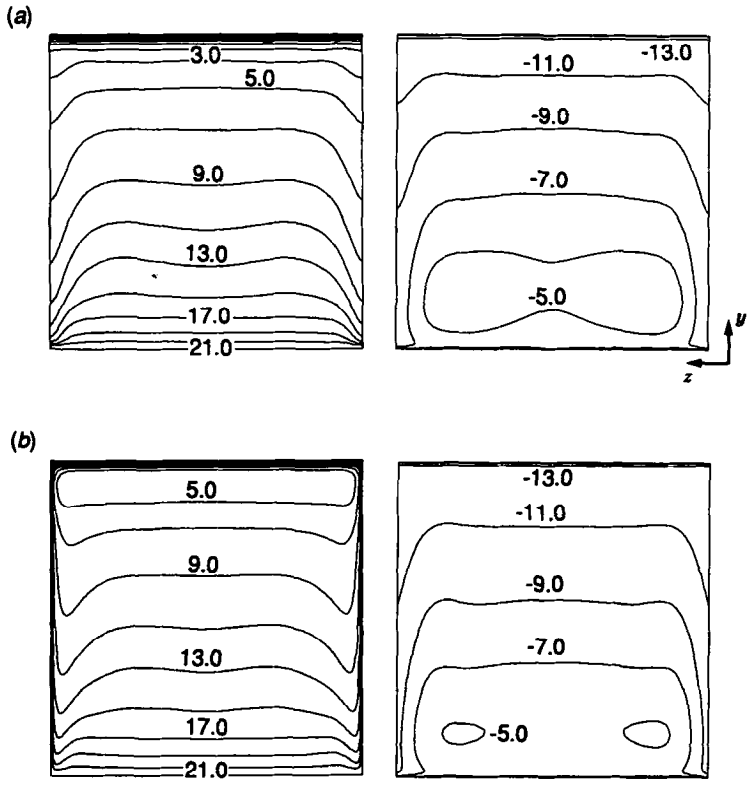

FIG. 3. The distribution of the local Nusselt number, Nu, at the heated wall ($x = 0$) (left) and at the cooled wall ($x = 1$) (right) for $Ra = 10^6$ and $T_c = 0.0$. (a) $S_y = 10.0$ and $S_z = 0.0$. (b) $S_y = 10.0$ and $S_z = 5.0$.

Table 1. The average Nusselt number, $\overline{Nu}$, at $Ra = 10^6$ ($S_z = 0.0$, $T_e = 0.5$)

S_y	0.0	1.0	5.0	10.0	∞
$\overline{Nu}\|_{x=0}$	8.675	8.459	8.159	8.144	6.678
$\Sigma(\overline{Nu} > 0)$	8.675	8.958	9.607	10.07	10.30

Note: $\overline{Nu}|_{x=1} = -\overline{Nu}|_{x=0}$; $\overline{Nu}|_{y=1} = \Sigma(\overline{Nu} > 0) - \overline{Nu}|_{x=0} = -\overline{Nu}|_{y=1}$.

Table 2. The average Nusselt number, $\overline{Nu}$, at $Ra = 10^6$ ($S_y = 10.0$)

S_z	0.0	5.0	5.0
T_e	0.0	0.0	0.5
$\overline{Nu}\|_{x=0}$	10.18	11.28	8.319
$\overline{Nu}\|_{x=1}$	−6.30	−5.30	−8.304
$\overline{Nu}\|_{y=0}$	−0.388	−0.204	−1.725
$\overline{Nu}\|_{y=1}$	−3.562	−2.90	1.732
$\overline{Nu}\|_{z=0}$	0.0	−1.437	0.0
$\Sigma(\overline{Nu} > 0)$	10.18	11.42	10.05

Note: $\overline{Nu}|_{z=0} = \overline{Nu}|_{z=1}$.

with respect to the cavity center. Figure 2(a) is for the reference case ($S_y = S_z = 0.0$), i.e. the perfectly insulated horizontal and end walls. As the thermal boundary layer near the heated wall develops from the bottom plate ($y = 0$) toward the ceiling ($y = 1$), the local Nusselt number varies significantly in the vertical direction. However, Nu is fairly uniform in the z-direction in much of the heated wall, except for the regions close to the end walls located at $z = 0$ and 1. When an appreciable heat transfer through the horizontal walls is allowed (for example, $S_y = 10.0$, as portrayed in Fig. 2(b)), the overall magnitude of Nu is reduced; this is obvious in view of the fact that a fraction of heat can now be transferred through the horizontal walls. No heat transfer takes place at the end walls ($z = 0$ and 1), which have the value of $S_z = 0.0$. When the end walls are also conductors, the features of iso-Nu contours are remarkably modified (compare Fig. 2(c) with Fig. 2(b)). Figure 2(d) shows the result obtained by imposing a linear temperature profile on the horizontal walls. This can be regarded as the limiting case for which $S_y \to \infty$. The magnitudes of Nu are reduced further since a large part of heat transfer (approximately 35% of the total incoming heat, see Table 1) occurs through the horizontal walls.

If the environment temperature is different from 0.5, the anti-symmetry of Nu patterns with respect to the cavity center disappears. For the results depicted in Fig. 3, T_e is set equal to the cooled wall temperature ($T_e = 0.0$). At the heated wall ($x = 0$), the qualitative features of the Nu distribution remain similar to the cases in which $T_e = 0.5$ (compare the corresponding results in Fig. 3(a) with Fig. 2(b), and Fig. 3(b) with Fig. 2(c)). At the cooled wall, however, the Nu patterns are drastically altered from those at the heated wall.

The average Nusselt numbers, $\overline{Nu}$, at the cavity walls are compiled in Tables 1 and 2. Table 1 represents the variation of $\overline{Nu}$ at the heated wall ($\overline{Nu}|_{x=0}$) and changes in the sum of the average Nusselt number for which $\overline{Nu} > 0$ ($\Sigma(\overline{Nu} > 0)$). The values of S_y are altered, while S_z and T_e are fixed at 0.0 (i.e. insulated end walls) and 0.5, respectively. Due to the aforementioned symmetry of the local Nusselt number distribution, $\overline{Nu}$ at the cooled wall ($\overline{Nu}|_{x=1}$) is equal to $-\overline{Nu}|_{x=0}$. The total sum of positive $\overline{Nu}$ is a measure of the magnitude of heat transfer between the fluid inside the cavity and the environment. As S_y increases, $\overline{Nu}|_{x=0}$ gradually decreases; on the other hand, $\Sigma(\overline{Nu} > 0)$ increases since the conducting horizontal wall at $y = 1$ enhances transport of heat into the cavity. At $S_y = 10.0$, approximately 20% of the positive $\overline{Nu}$ is found to occur at that horizontal wall.

Table 2 summarizes $\overline{Nu}$ at different walls for various values of S_z and T_e and for $S_y = 10.0$. When T_e is equal to the cooled wall temperature ($T_e = 0.0$), the heat transfer patterns at the two side walls are not symmetric, i.e. $\overline{Nu}|_{x=1} \neq -\overline{Nu}|_{x=0}$. In this case, a considerable amount of heat is seen to be removed from the cavity through the wall at $y = 1$. It is also evident that heat leaves the cavity from all of the conducting surfaces except for the heated wall, since the environmental temperature T_e is always lower than or equal to the fluid temperature. If T_e is maintained at 0.5, the energy balance at each end wall is always satisfied irrespective of the value of S_z due to the symmetry of the field that arises inside the cavity.

In order to examine further the local changes in the fields, the profiles of the velocity components and of the temperature at the plane of symmetry ($z = 0.5$) are inspected.

In Fig. 4, the u-velocity profiles along the vertical line

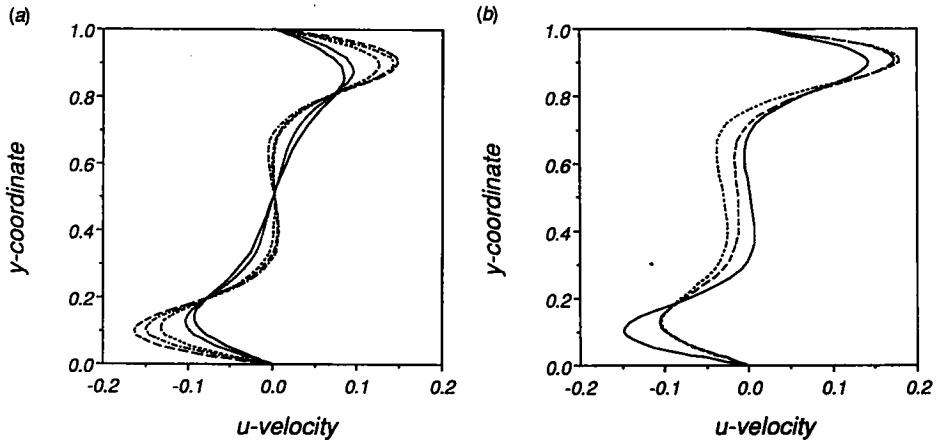

FIG. 4. Profiles of the u-velocity component in the mid-z-plane ($z = 0.5$) along the vertical line $x = 0.5$ for $Ra = 10^6$. (a) Effects of S_y (in all cases, $S_z = 0.0$ and $T_e = 0.5$). (——) $S_y = 0.0$; (····) $S_y = 1.0$; (– – –) $S_y = 5.0$; (–·–·–) $S_y = 10.0$; (– – –) $S_y \to \infty$. (b) Effects of S_z and T_e($S_y = 10.0$). (——) $S_z = 0.0$ and $T_e = 0.5$; (– – –) $S_z = 0.0$ and $T_e = 0.0$; (---) $S_z = 5.0$ and $T_e = 0.0$.

$x = 0.5$ are plotted. When $S_z = 0.0$ and $T_c = 0.5$ (Fig. 4(a)), the profiles are anti-symmetric with respect to $y = 0.5$, as anticipated. Due to the heat transfer at the horizontal walls ($y = 0$ and 1), the peak values of u increase as S_y increases. When $S_y = 10.0$, the velocity profile is shown to be almost similar to that of the limiting case, $S_y \to \infty$. If T_c is equal to the cooled wall temperature ($T_c = 0.0$), flows near the top horizontal wall ($y = 1$) are accelerated, as illustrated in Fig. 4(b). Heat transfer from the end walls is shown to strengthen this activity and, at the same time, it induces flows of appreciable magnitude in the central portion of the cavity.

The temperature profiles at various y locations are displayed for selected combinations of S_y, S_z and T_c in Fig. 5. In the case of $S_y = 10.0$, $S_z = 0.0$ and $T_c = 0.5$, the overall temperatures attain higher values in $y < 0.5$ than those of the reference case ($S_y = S_z = 0.0$ and $T_c = 0.5$); this trend is reversed in $y > 0.5$. Near the bottom plate at $y = 0$ (or the ceiling at $y = 1$) flows of high (low) temperatures tend to penetrate to the cavity interior when heat transfer is present at the horizontal walls. Under the condition of $S_y = 10.0$, $S_z = 0.0$ and $T_c = 0.0$, deviations from the reference case are pronounced as y increases since the heat loss from the ceiling is larger than that occurring at the floor. If, further, S_z is set equal to 5.0, departures from the reference adiabatic wall case become further pronounced.

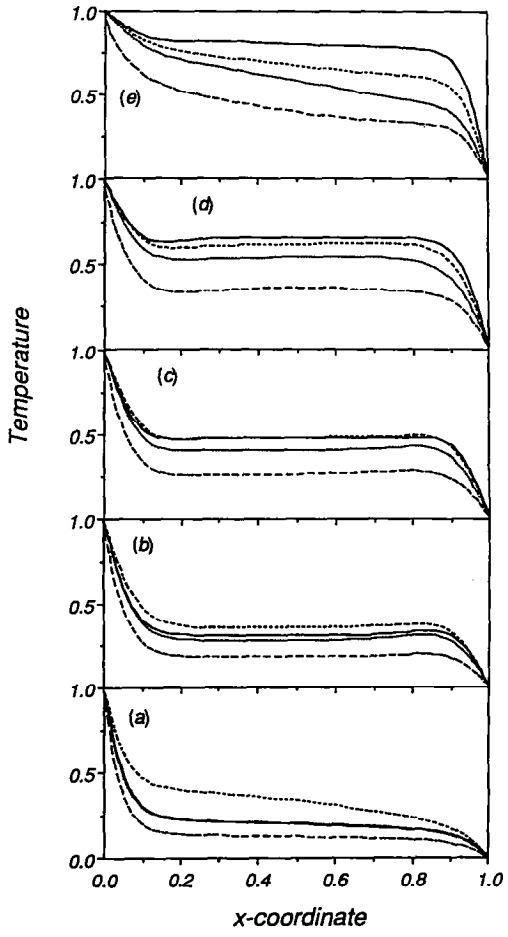

FIG. 5. Distribution of the temperature in the mid-z-plane ($z = 0.5$) at various heights of $Ra = 10^6$. (——) $S_y = S_z = 0.0$ and $T_c = 0.5$; (– – –) $S_y = 10.0$, $S_z = 0.0$ and $T_c = 0.5$; (····) $S_y = 10.0$, $S_z = 0.0$ and $T_c = 0.0$; (– · –) $S_y = 10.0$, $S_z = 5.0$ and $T_c = 0.0$. (a) $y = 0.1$. (b) $y = 0.3$. (c) $y = 0.5$. (d) $y = 0.7$. (e) $y = 0.9$.

CONCLUDING REMARKS

Effects of the partially conducting surface walls of a differentially heated cubical enclosure are studied numerically. By utilizing the present thermal conductance model, it is demonstrated that the overall flow and heat transfer activities are enhanced. When the horizontal walls have finite conductance of $S_y \leqslant 10.0$, an appreciable heat transfer takes place in the vertical direction. If the environmental temperature is equal to that of the cooled wall, asymmetry is remarkable in the fields.

REFERENCES

1. S. Ostrach, Natural convection in enclosures, *J. Heat Transfer* **110,** 1175–1190 (1988).
2. G. de Vahl Davis, Natural convection of air in a square cavity: a bench mark numerical solution, *Int. J. Numer. Meth. Fluids* **3,** 249–264 (1983).
3. T. Saitoh and K. Hirose, High-accuracy bench mark solutions to natural convection in a square cavity, *Comput. Mech.* **4,** 417–427 (1989).
4. P. Le Quéré, Accurate solutions to the square thermally driven cavity at high Rayleigh number, *Comput. Fluids* **20,** 29–41 (1991).
5. E. I. Lee and V. Sernas, Numerical study of heat transfer in rectangular air enclosure of aspect ratio less than one, ASME Paper No. 80-WA/HT-43 (1980).
6. P. Le Quéré and T. A. de Roquefort, Transition to unsteady natural convection of air in vertical differentially heated cavities: influence of thermal boundary conditions on the horizontal walls, *Proc. 8th Int. Heat Transfer Conf.* **4,** 1533–1538 (1986).
7. R. A. W. M. Henkes and C. J. Hoogendoorn, Bifurcation to unsteady natural convection for air and water in a cavity heated from the side, *Proc. 9th Int. Heat Transfer Conf.* **2,** 257–262 (1990).
8. D. M. Kim and R. Viskanta, Study of the effects of wall conductance on natural convection in differentially oriented square cavities, *J. Fluid Mech.* **144,** 153–176 (1984).
9. L. Rahm and G. Walin, On thermal convection in stratified fluids, *Geophys. Astrophys. Fluid Dyn.* **13,** 51–65 (1979).
10. J. M. Hyun, Convection in a rotating cylinder with its sidewall having a finite thermal conductance, *Geophys. Astrophys. Fluid Dyn.* **34,** 83–98 (1985).
11. Y. Le Pentrec and G. Lauriat, Effects of the heat transfer at the side walls on natural convection in cavities, *J. Heat Transfer* **112,** 370–378 (1990).
12. T. Fusegi, J. M. Hyun, K. Kuwahara and B. Farouk, A numerical study of three-dimensional natural convection in a differentially heated cubical enclosure, *Int. J. Heat Mass Transfer* **34,** 1543–1557 (1991).
13. C. J. Freitas, R. L. Street, A. N. Findikakis and J. R. Koseff, Numerical simulation of three-dimensional flow in a cavity, *Int. J. Numer. Meth. Fluids* **5,** 561–575 (1985).
14. S. V. Patankar, *Numerical Heat Transfer and Fluid Flow*, Chap. 6. Hemisphere, Washington, DC (1980).
15. H. L. Stone, Iterative solution of implicit approximations of multi-dimensional partial differential equations, *J. Numer. Anal.* **5,** 530–558 (1968).